Journal of Hazardous Materials 328 (2017) 90–97

Contents lists available at ScienceDirect

Journal of Hazardous Materials

journal homepage: www.elsevier.com/locate/jhazmat

Stable isotope composition of mercury forms in flue gases from a typical coal-fired power plant, Inner Mongolia, northern China

Shunlin Tang[a,*], Chaohui Feng[a], Xinbin Feng[b], Jianming Zhu[a,c], Ruoyu Sun[d,*], Huipeng Fan[a], Lina Wang[a], Ruiyang Li[a], Tonghua Mao[a], Ting Zhou[e]

[a] Institute of Resources and Environment, Henan Polytechnic University, Jiaozuo, Henan Province, 454000, China
[b] State Key Laboratory of Environmental Geochemistry, Institute of Geochemistry, Chinese Academy of Sciences, Guiyang, 550002, China
[c] State Key Laboratory of Geological Processes and Mineral Resources, China University of Geosciences, Beijing, 100086, China
[d] CAS Key Laboratory of Crust-Mantle Materials and Environment, School of Earth and Space Sciences, University of Science and Technology of China, Hefei, Anhui 230026, China
[e] State Key Laboratory of Ore Deposit Geochemistry, Institute of Geochemistry, Chinese Academy of Sciences, Guiyang, 550002, China

HIGHLIGHTS

- The first speciated Hg isotope ratios in coal combustion flue gases are presented.
- Significant Hg isotope kinetic MDF was observed during Hg forms transformation.
- Emitted gaseous Hg highly enriches in heavy Hg isotopes relative to feed coal.

GRAPHICAL ABSTRACT

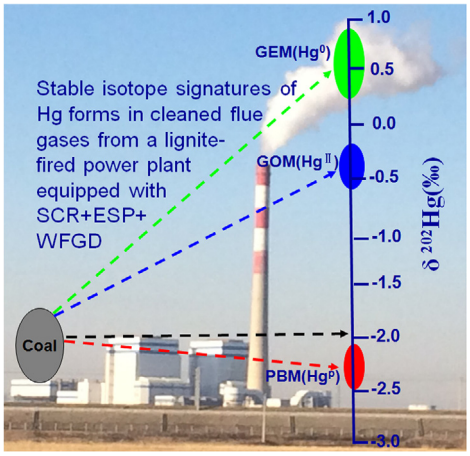

ARTICLE INFO

Article history:
Received 8 December 2016
Received in revised form 8 January 2017
Accepted 10 January 2017
Available online 11 January 2017

Keywords:
Mercury isotope
Mercury forms
Coal-fired power plant
Mass dependent fractionation

ABSTRACT

Mercury forms emitted from coal combustion via air pollution control devices are speculated to carry different Hg isotope signatures. Yet, their Hg isotope composition is still not reported. Here, we present the first onsite Hg isotope data for gaseous elemental Hg (GEM) and gaseous oxidized Hg (GOM) of flue gases from a typical lignite-fired power plant (CFPP). Significant mass dependent fractionation (MDF) and insignificant mass independent fractionation (MIF) are observed between feed coal and coal combustion products. As compared to feed coal ($\delta^{202}Hg = -2.04 \pm 0.25‰$), bottom ash, GEM and GOM in flue gases before and after wet flue gas desulfurization system significantly enrich heavy Hg isotopes by 0.7–2.6‰ in $\delta^{202}Hg$, while fly ash, desulfurization gypsum and waste water show slight but insignificant enrichment of light Hg isotopes. GEM is significantly enriched heavy Hg isotopes compared to GOM and Hg in fly ash. Our observations verify the previous speculation on Hg isotope fractionation mechanism in CFPPs, and

* Corresponding authors.
E-mail addresses: tangshunlin@hpu.edu.cn (S. Tang), ruoyu.sun@tju.edu.cn (R. Sun).

http://dx.doi.org/10.1016/j.jhazmat.2017.01.014

suggest a kinetically-controlled mass dependent Hg isotope fractionation during transformation of Hg forms in flue gases. Finally, our data are compared to Hg isotope compositions of atmospheric Hg pools, suggesting that coal combustion Hg emission is likely an important atmospheric Hg contributor.

1. Introduction

Mercury (Hg) is a toxic pollutant, which is released from both natural and anthropogenic sources [1–3]. Hg emitted from natural sources is thought to be mainly in the form of gaseous elemental Hg (GEM), whereas anthropogenically emitted Hg has a large portion of gaseous oxidized mercury (GOM) and particle-bound mercury (PBM) [4]. GEM has a relatively long atmospheric residence time (~1 year), and can be transported globally [4,5]. GOM and PBM are readily scavenged from atmosphere, and deposit in the vicinity of emission sources [4,6]. Modern industrialization has increased Hg loading into the surface environment by a factor of 2–5 [7,8]. Coal combustion is the main anthropogenic Hg source, reaching 700–900 tons/year into atmosphere [1,2,9]. Coal-fired power plants are considered to be the largest point Hg sources in most countries. However, the identification and quantification of Hg emitted from coal-fired power plants are still challenged.

Mercury stable isotope has a potential in tracing sources of Hg and geochemical processes [10–13]. A series of physicochemical reactions involving Hg, such as biotic and photochemical reduction [14–18], methylation [19–21], demethylation [22,23], volatilization [24], evaporation [25,26], and adsorption [27,28] can systematically seperate Hg isotopes via mass dependent fractionation (MDF) and mass independent fractionation (MIF). Previous studies have shown >10‰ variations in both MDF (indicated by δ^{202}Hg) and MIF of odd Hg isotopes (indicated by Δ^{199}Hg) in natural samples [10,29–33].

Biswas et al. [34] first showed that the MDF and MIF signatures of Hg isotopes in coal could be used as a diagnostic tool for "fingerprinting" Hg emissions from different coal sources by using a step heating combustion procedure to preconcentrate Hg in an oxidizing solution of 1% $KMnO_4$ and 1.8 M H_2SO_4. The distinguishability of different world regional coals by Hg isotope composition is further explored in Sun et al. [35] However, the air pollution control devices(APCDs) and speciated Hg conversion process possibly shifts the isotope composition of emitted Hg relative to combusted coal [35,36]. This would obscure the source tracing of Hg emissions from coal combustion [37,38]. By measuring Hg isotope composition in feed coal and its combustion products (i.e., bottom ash, fly ash and desulfurization gypsum), Sun et al. [36] estimated that the emitted total Hg from a typical CFPP enriched heavy Hg isotopes by ~0.3‰ in δ^{202}Hg relative to feed coal, and suggested that different Hg species in CFPP flue gasses might carry contrasting MDF signatures. Further, Sun et al. [35] developed a double-Rayleigh MDF model for Hg species in CFPP flue gasses, and predicted that GEM is enriched heavy isotope compared to GOM and PBM. Similarly, significant isotope fractionation is also observed in CFPP for other elements like S and Zn [39,40]. Direct Hg isotope measurement on different Hg species in CFPP flue gases is still lacking, which limit our ability to trace the contribution of coal combustion in atmospheric Hg pools [41–43].

In this study, we present the first onsite Hg isotope measurement on gaseous Hg (GEM and GOM) in flue gases of a CFPP from Inner Mongolia, North China. Our aims are to: (1) examine speciated Hg isotope shifts of coal combustion emissions relative to feed coal; (2) understand Hg isotope fractionation mechanisms during coal combustion and transport of flue gases through post-combustion APCDs; (3) test if the previous CFPP Hg isotope fractionation models can correctly predict our observations on Hg forms.

2. Experimental section

2.1. Configuration of CFPP and sampling sites

The sampling was carried out in a typical 300 MW subcritical CFPP fed by pulverized lignite in a power plant, Mongolian, China. The studied CFPP is installed with a selective catalytic reduction system (SCRs) to control NOx emissions, followed by electrostatic precipitators (ESPs) to remove particles and wet limestone flue gas desulfurization systems (WFGD) to control SO_2 emissions. During the sampling period, the studied CFPP was operated under normal conditions. The configuration of the studied CFPP and sampling sites are showed in Fig. 1.

2.2. Sampling and processing

A C-5000 source sampling system (Environmental Supply Company, USA) was used to sample Hg forms in flue gases at the inlet and outlet of WFGD according to the Ontario Hydro Method [44] in the field because of high percentage of PBM in flue gas before the ESPs that can be absorbed on the filter and seriously affected mercury forms of the sampling flue gas and frequently blocked the sampling device. The Hg forms in coal combustion flue gases were withdrawn iso-kinetically into the sampling train through a probe/filter system maintaining at 120 °C. PBM was recovered from the particle captured in the filter. However, due to >99.6% particle removal efficiency of ESPs for the studied power plant[45], we did not collect enough particle samples on the filter for Hg isotope measurement. Gaseous Hg was collected in the sampling train composed of a series of impingers in an ice bath at the inlet (i) and outlet (o) of WFGD. The first three impingers filled with 1.0 mol/L KCl solution were used to collect GOM. GEM is collected in the subsequent impingers including one impinger containing a mixture of 5% HNO_3 and 10% peroxide H_2O_2, and three impingers, each containing a mixture of 4% $KMnO_4$ and 10% H_2SO_4 [34,37]. After each sampling campaign, the three combined KCl solution, one $HNO_3-H_2O_2$ solution and three combined $H_2SO_4+KMnO_4$ solution were immediately transferred into three 250 ml pre-cleaned boron silicon glass bottles as GOMi/o (KCl), GEMi/o (HNO_3–H_2O_2) and GEMi/o ($KMnO_4$–H_2SO_4), respectively. The Hg concentrations in collected solutions were initially measured in the field by Lumex R915 M. According the results, we adjusted appropriate sampling flow rates and sampling time to collect enough Hg for isotope measurement.

Feed coal was sampled from the pneumatic conveying duct connected to the CFPP. Limestone and fresh processing water were collected from the inlet of WFGD. Bottom ash from the grate below the boiler, fly ash from all hoppers of ESPs, desulfurization gypsum and desulfurization recycling waste water for WFGD, were collected shortly after combustion of feed coal. The solid samples were stored in polyethylene bags, and water samples were stored in 1 l PTFE bottles. The sampling frequency of solid and water samples (generally 2–3 times a day) was determined by the sampling arrangement of the flue gases. The total sampling duration is

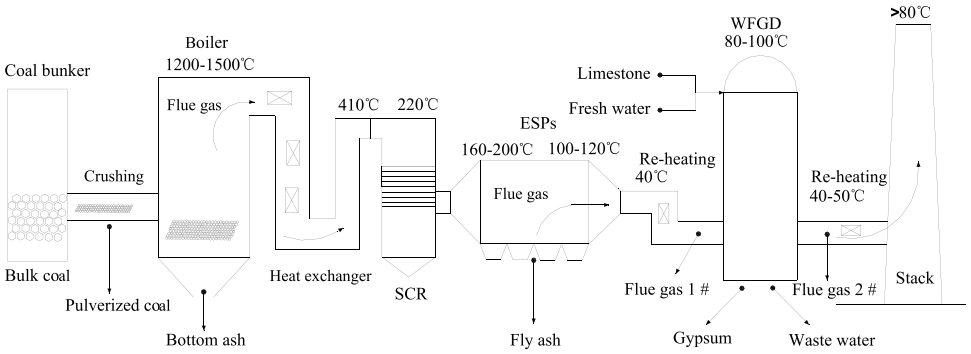

Fig. 1. Configuration of the studied CFPP and sampling sites (●).

4–5 days. All the solid samples including feed coal, bottom ash, fly ash and gypsum were dried in a fume hood to a constant weight, and then milled and sieved to 200 meshes. Appropriate amounts of powdered solid samples were weighted into 45 ml centrifugal tubes, and digested using the mixture acid. We used 10 ml aqua regia (HNO_3: HCl = 1:3, v:v) to digest solid samples except coal samples. For coal digestion, we used 10 ml reverse aqua regia (HNO_3: HCl = 3:1, v:v) because of the high content of organic matters in coal. The centrifugal tubes of digested samples were shaken overnight before placing them in a water bath. The water bath is first kept at 50 °C for half an hour, and then heated to 95 °C holding for 2 h. Following cooling down to room temperature, sample digests were filtrated into new 45 ml centrifugal tubes using disposable syringes and syringe-driven 0.45 μm PVDF filters (Millex, OD = 33 mm). The filtered sample digests were capped, labeled and stored in a refrigerator. For the desulfurization recycling waste water, ~10 ml of sample was transferred into a 45 ml centrifugal tube, and then digested using 100 μl BrCl for 2 h. The GEMi/o ($KMnO_4$–H_2SO_4) solutions were reduced with appropriate quantities of NH_2OH-HCl (30%, w/v) to dissolve purple Mn precipitates prior to subsequent analysis.

Two-stage combustion furnaces with a custom-made continuous quartz glass combustion [46] were connected to the front of the C-5000 source sampling system for testing mercury recovery of our field sampling system and method in laboratory. Quartz boat with NIST SRM 3133(5 ml, 100 ppb) solution and a coal sample from this study with known Hg concentration were placed within the first furnace, and were heated from 25 °C to 750 °C over 7 h during a series of ramp and the decomposition furnace was held at 1000 °C for the duration of the procedure, respectively. A flow of ~6 L/min Hg-free air (gold trapping at the inlet of quartz tube) was introduced into the combustion tube furnace. The solutions recovered as same as the field sampling were analyzed for Hg concentration and Hg isotope ratio.

2.3. Hg concentration analysis and Hg isotope ratio measurement

The Hg concentrations in sample solutions of GOMi/o (KCl), GEM i/o (HNO_3–H_2O_2) and GEMi/o ($KMnO_4$–H_2SO_4) sample, and in sample digestions of feed coal, bottom ash, fly ash, gypsum and waste water were analyzed with a CV-AFS (Brooks Rand Model III) and has been reported previously [45].

In view of the analyzed Hg concentration, the sample solutions/digestions were diluted to 1 and 2 ng mL^{-1} using Milli-Q water (18.2 MΩ cm^{-1}) to match the concentrations (1 and 2 ng/ml) of NIST SRM 3133 Hg standard solutions within 5%. Mercury isotope ratio was determined by a MC-ICPMS (NEPTUNE Plus) at the State Key Laboratory of Ore Deposit Geochemistry, CAS, China. The sample Hg^{II} was reduced into Hg^0 vapor by $SnCl_2$ (3%, w/w, in 20% HCl) in a continuous flow cold vapor generator (CV) (HGX-200, CETAC), and then introduced into plasma sources with Tl aerosol generated by a desolvation unit (Apex-Q, Elemental Scientific Inc). Instrumental mass bias was corrected using internal Tl standard by assuming an exponential fractionation law and a reference $^{205}Tl/^{203}Tl$ value of 2.38714, and standard-sample-standard bracketing method. Data were acquired by monitoring voltage signals of ^{198}Hg, ^{199}Hg, ^{200}Hg, ^{201}Hg, ^{202}Hg, ^{203}Tl and ^{205}Tl for a period of 10 min (1 block, 100 cycles, 6 s integration time). Instrument blanks were measured following each sample and bracketed NIST SRM 3133 standard, and subtracted online. Typical blank values were <10 mV for ^{202}Hg which is insignificant compared to typical sample and standard ^{202}Hg signals. The sample solutions of 1 and 2 ng mL^{-1} gave typical ^{202}Hg signals of 0.8–0.9 V and 1.7–1.8 V, respectively.

Mercury isotope ratios are reported in delta (δ) notation representing per mil deviations of samples from NIST SRM 3133 Hg standard [47]:

$$\delta^{202}\mathrm{Hg}(‰) = \left[\left(^{xxx}\mathrm{Hg}/^{198}\mathrm{Hg}\right)_{\mathrm{sample}} / \left(^{xxx}\mathrm{Hg}/^{198}\mathrm{Hg}\right)_{\mathrm{NIST3133}} - 1\right] \times 1000 \quad (1)$$

Where xxx is the mass of Hg isotopes between 199 and 202. MIF is reported in capital delta notation (Δ^{xxx}Hg), which represents the deviation of measured δ^{xxx} Hg from that theoretically predicted by δ^{202}Hg using the mass dependent law [47]:

$$\Delta^{xxx}\mathrm{Hg}(‰) = \delta^{xxx}\mathrm{Hg} - \beta_{xxx} \times \delta^{202}\mathrm{Hg} \quad (2)$$

The mass dependent scaling factor β_{xxx} is 0.2520 for ^{199}Hg, 0.5024 for ^{200}Hg, 0.7520 for ^{201}Hg and 1.4930 for ^{204}Hg.

2.4. Recovery and uncertainty

Acid digestion of coal standards (NIST SRM 2692C and 2693) satisfied >80% Hg recovery. The ratio of Hg input/output of the tested combustion is 92% for Apr. 25 and the Hg mass balance during our sampling period is 110% for mean Hg after passing through SCR, ESP and WFGD [45]. Typical internal precision of Hg isotope ratio (e.g. $^{202}Hg/^{198}Hg$) measurement was below 0.05‰ (1 SE) for individual sample analysis. The long-term analytical uncertainty of the method was determined by repeated analyses of the UM-Almadeín standard solutions of 1.0 or 2.0 ng/g Hg. The average values are −0.57 ± 0.08‰ (2SD, n = 9) for δ^{202}Hg, −0.02 ± 0.06‰ (2SD, n = 9) for Δ^{199}Hg and −0.05 ± 0.06‰ (2SD, n = 9) for Δ^{201}Hg (Table S1), which are consistent with previously reported values [46,47]. The combusted NIST SRM 3133 Hg recovery ranged from 92.8 to 113.4% (103.0 ± 9.1%, 1SD, n = 4), among which 89.8–94.6% was absorbed by the first impinge with mixture solutions of 4% $KMnO_4$ and 10% H_2SO_4. The Hg recovery of the combusted coal in the two-stage combustion furnace was 100.6%.

The Hg concentrations in GEM i/o (HNO_3–H_2O_2) solutions, PBM digestions, limestone, process water and some bottom ash samples

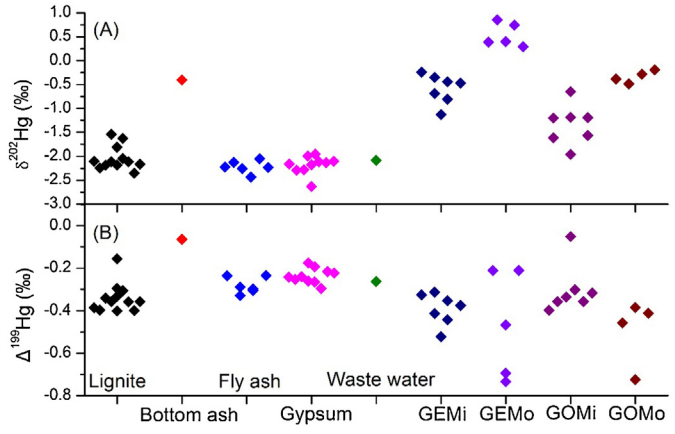

Fig. 2. Variations of δ^{202}Hg (A, upper panel) and Δ^{199}Hg (B, lower panel)in feed coal and its combustion products including bottom ash, fly ash, gypsum, waste water, GEMi and GOMi in flue gases before WFGD and GEMo and GOMo in flue gases after WFGD in a lignite-fired utility boiler. The typical 2SD analytic uncertainty is 0.08‰ for δ^{202}Hg and 0.06‰ for Δ^{199}Hg.

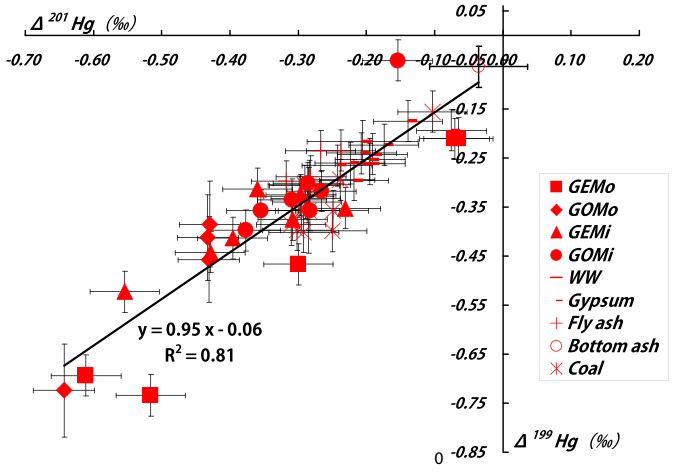

Fig. 3. Regression line of Δ^{201}Hg vs. Δ^{199}Hg in feed coal and its combustion products (bottom ash, fly ash, gypsum, WW-waste water, GEM and GOM in flue gases before and after WFGD) in a lignite–fired utility boiler.

are too low, thus are not analyzed for Hg isotope ratios. Uncertainties of Hg isotope ratios reported in this study correspond to the larger value of either (1) the external 2SD uncertainty of repeated measurements of the UM-Almadeín or (2) the 2SD uncertainty of replicate analysis of samples.

3. Results and discussion

3.1. Hg isotope MDF and MIF in coal and coal combustion products

We observe as large as 3.5‰ variation in δ^{202}Hg (−2.63‰ to 0.85‰) in feed lignite and its combustion products including bottom ash, fly ash, desulfurization gypsum, desulfurization recycling waste water, GEM and GOM in flue gases before and after WFGD (Fig. 2A; Table S2). Relative to δ^{202}Hg of the feed lignite (−2.04 ± 0.25‰, 1SD, n = 12), a single bottom ash is significantly enriched in heavier Hg isotopes by 1.6‰ (−0.41 ± 0.04‰, 1SD, n = 1), while fly ash (−2.22 ± 0.13‰, 1SD, n = 6), desulfurization gypsum (−2.18 ± 0.19‰, 1SD, n = 10) and one desulfurization waste water sample (−2.09 ± 0.04‰, 1SD, n = 1) show slight but insignificant depletion ($p > 0.05$) of heavy Hg isotopes (Fig. 2A, Table 1). The GOM and GEM in the flue gases at inlet of WFGD (GOM_i = −1.34 ± 0.42‰, 1SD, n = 7; GEM_i = −0.59 ± 0.31‰, 1SD, n = 7) and outlet of WFGD (GOM_o = −0.34 ± 0.13‰, 2SD, n = 4; GEM_o = 0.54 ± 0.25‰, 2SD, n = 5) have the highest δ^{202}Hg values, significantly enriching heavier Hg isotopes compared to feed lignite and coal combustion products including fly ash, desulfurization gypsum and waste water. Moreover, GEM is enriched in heavier Hg isotopes by ~0.8‰ in δ^{202}Hg than GOM in flue gases before (GEM_i-GOM_i = 0.75 ± 0.52‰, $p < 0.01$) and after WFGD (GEM_o-GOM_o = 0.87 ± 0.28‰, $p < 0.01$). After the flue gases passing through the WFGD, both GEM (GEM_o-GEM_i = 1.13 ± 0.39‰, $p < 0.01$) and GOM (GOM_o-GOM_i = 1.00 ± 0.44‰, $p < 0.01$) show >1.0‰ enrichment of heavier Hg isotopes in δ^{202}Hg (Fig. 2A, Table 1). The statistical difference in mean δ^{202}Hg between feed coal and its combustion products, and between Hg forms in flue gases suggest that significant MDF occurs during the combustion of feed coal and the subsequent transport and conversion of Hg forms in post-combustion flue gases. Sun et al. [36] also observed up to 2‰ variation in δ^{202}Hg between feed coal and coal combustion products (bottom ash, fly ash and gypsum).

Despite 0.7‰ variation (−0.73‰ to 0.01‰) in Δ^{199}Hg in feed lignite and its combustion products are observed, there are no significant difference in mean Δ^{199}Hg ($p > 0.05$) between feed lignite and its combustion products except gypsum and fly ash ($\Delta^{199}Hg_{gypsum} - \Delta^{199}Hg_{lignite}$ = 0.10 ± 0.08‰, $\Delta^{199}Hg_{flyash} - \Delta^{199}Hg_{lignite}$ = 0.06 ± 0.08‰, 1SD, $p < 0.05$) (Table 1). Nearly all of the studied samples are characterized by significant negative MIF values (Fig. 2B, Table S2), with Δ^{199}Hg as low as −0.7‰. The feed lignite samples have a mean Δ^{199}Hg of −0.34 ± 0.07‰ (1SD, n = 12), varying from −0.40‰ to −0.16‰. A linear regression of Δ^{199}Hg vs. Δ^{201}Hg for all samples yield a slope of 0.95 ± 0.12 (2SE, r^2 = 0.91, $p < 0.01$) (Fig. 3), which is comparable to the slope of world coal deposits (1.07 ± 0.04, 2SE) [29]. It suggests that the MIF signatures in coal combustion products are probably inherited from feed coal rather than generated by combustion Hg transformation processes [36]. The small MIF difference (<0.10‰ in Δ^{199}Hg) between fly ash/gypsum and lignite (Table 1) might relate to the natural variation of Δ^{199}Hg in lignite that is not fully accounted in our lignite samples. In the following, we first evaluate the MDF Hg isotope balance of the studied CFPP, and then discuss in detail the combustion physicochemical processes that control MDF in feed coal and its combustion products.

3.2. Mercury and Hg isotope mass balance

Mercury and Hg isotope mass balance of the studied CFPP are calculated at both inlet and outlet of WFGD to evaluate our sampling protocols and analytic accuracy. The calculation details are presented in supporting information. The Hg mass balance at inlet and outlet of WFGD and the input/output Hg ratio is 86 ± 25% (1SD) at the inlet of WFGD and is 110 ± 31% at the outlet of WFGD [45]. Mercury isotope mass balance is evaluated by comparing the calculated δ^{199}Hg and Δ^{199}Hg values of feed coal with those materials measured by MC-ICPMS. The calculated feed coal δ^{202}Hg and Δ^{199}Hg are −1.92 ± 0.58‰ (1SD) and −0.36 ± 0.58‰ (1SD) for Hg isotope mass balance before WFGD, and −1.47 ± 0.43‰ (1SD) and −0.29 ± 0.10‰ (1SD) for Hg isotope mass balance after WFGD. These values are statically same as those measured by MC-ICPMS for feed coal (δ^{202}Hg = −2.04 ± 0.25‰, Δ^{199}Hg = −0.34 ± 0.07‰, 1SD, Table 1) except δ^{202}Hg calculated using Hg isotope mass balance after WFGD (See supporting information for explanation).

3.3. Hg isotope composition in feed coal (lignite)

The feed lignite samples of studied CFPP were from Xilinguole, Inner Mongolia, one of the two largest lignite producing

Table 1
Summary of δ^{202}Hg (‰) and Δ^{199}Hg (‰) of feed coal and coal combustion products, and their distinguishability based on *t*-test.

	δ^{202}Hg	1SD	p value(*t*-test)	Δ^{199}Hg	1SD	p value(*t*-test)
Lignite	−2.04	0.25		−0.34	0.07	
Bottom ash	−0.41	0.04		−0.06	0.03	
Fly ash	−2.22	0.13		−0.28	0.04	
Gypsum	−2.18	0.19		−0.24	0.04	
Waste water	−2.09	0.04		−0.26	0.03	
GEMi	−0.59	0.31		−0.39	0.07	
GOMi	−1.34	0.42		−0.30	0.11	
GEMo	0.54	0.25		−0.46	0.25	
GOMo	−0.34	0.13		−0.49	0.16	
Bottom ash- Lignite	1.63	0.25		0.28	0.07	
Fly ash- Lignite	−0.18	0.28	0.06	0.06	0.08	0.03
Gypsum- Lignite	−0.14	0.31	0.14	0.10	0.08	0.00
Waste water- Lignite	−0.05	0.25		0.08	0.07	
GEMi-Lignite	1.45	0.39	0.00	−0.05	0.10	0.15
GOMi-Lignite	0.70	0.49	0.00	0.04	0.13	0.45
GEMo- Lignite	2.58	0.35	0.00	−0.12	0.26	0.34
GOMo- Lignite	1.70	0.28	0.00	−0.15	0.17	0.14
GEMi-GOMi	0.75	0.52	0.00	−0.09	0.14	0.11
GEMo-GOMo	0.87	0.28	0.00	0.03	0.30	0.83
GEMo-GEMi	1.13	0.39	0.00	−0.07	0.26	0.57
GOMo-GOMi	1.00	0.44	0.00	−0.19	0.19	0.08

regions in China. Lignite samples are characterized by slightly negative Δ^{199}Hg (-0.34 ± 0.07‰, 1SD, n = 12, from −0.40‰ to −0.16‰) and moderately negative δ^{202}Hg(-2.04 ± 0.25‰, 1SD, n = 12, from −2.35‰ to −1.54‰). Relative to the world lignite (δ^{202}Hg = -1.43 ± 0.74‰, Δ^{199}Hg = -0.19 ± 0.23‰, 1SD, n = 18) [29], our lignite samples are significantly ($p < 0.02$) depleted heavy and odd Hg isotopes. Large variations in δ^{202}Hg (−3.90‰ to 0.77‰) and Δ^{199}Hg (−0.63‰ to 0.34‰) have been found across global coal deposits, and are interpreted to be controlled by biogenic Hg from terrestrial plants (37%–46%) and geogenic Hg from sediment sources (54%–63%)[29]. As suggested by Yin et al. [48], the low-rank coal from northwestern China mainly inherited biogenic Hg from coal-forming plants due to their low metamorphism.

3.4. Hg isotope composition in bottom ash

Our one single bottom ash sample exhibits high δ^{202}Hg of -0.41 ± 0.04‰ (1SD, n = 1) and insignificant Δ^{199}Hg of -0.06 ± 0.03‰ (2SD, n = 1). Relative to feed coal, δ^{202}Hg and Δ^{199}Hg are positively shifted by 1.6‰ and 0.3‰ (Table 1). During coal combustion, the vast majority (>99.5%, Table S3) of Hg in feed lignite is volatilized, leaving trace amounts of Hg in bottom ash. As shown previously, no MIF occurs during the high temperature industrial combustion and smelting processes [30,36,49–51]. The significant MIF shift of bottom ash relative feed coal indicates that there are at least two Hg pools in feed lignite. As proposed by Sun et al. [29] Hg in coal is broadly controlled by two sources: coal-forming plants characterized by lower and negative δ^{202}Hg and Δ^{199}Hg and source sediments characterized by higher δ^{202}Hg and near-zero Δ^{199}Hg. The source sediments are assigned with a δ^{202}Hg of -0.78 ± 0.51‰ (1SD) and Δ^{199}Hg of 0.00 ± 0.08‰ (1SD) based on bulk crustal rock [29]. Both values are comparable to the Hg isotope composition of our bottom ash. Therefore, we speculate that the Hg retained in the bottom ash might represent trace amounts of source sediment Hg (possibly incorporated into refractory minerals) that are not totally volatilized during coal combustion.

3.5. Hg isotope MDF in fly ash from ESPs

Mercury volatilized from coal under the high temperature (1200–1500 °C) of the boiler is mainly in form of GEM. The generated GEM is then transported downward along the flue gas duct where it is converted into GOM and PBM with the participation of various oxidants (e.g., Cl, Br, SO_x) and fly ash due to the decrease of temperate in the flue gases [52,53]. After entering into SCR, Hg forms are transformed again by the catalysts in the SCR. Subsequently, the coal flue gases are transported through ESPs and WFGD before emitting into atmosphere.

The fly ash collected in ESPs shows slight but insignificant enrichment of light Hg isotopes in δ^{202}Hg relative to the feed coal (Table 1). Sun et al. [36] found that relative to the feed coal, fly ash is significantly enriched light Hg isotopes by ~0.8‰ in δ^{202}Hg, with the enrichment trend decreasing with the decrease of particle size and collection temperature of fly ash. Our bulk fly ash samples are a mixture of fly ash collected from six ESPs hoppers, thus, we can not compare Hg isotope composition of fly ash with different particle size and collected at different temperature. The insignificantly small negative shift of δ^{202}Hg in our fly ash samples possibly relates to characteristics of feed coal (lignite) and the configurations of APCDs. Our studied CFPP was installed with SCR to control NOx emissions, which is absent in Sun et al. [36]. When the coal combustion flue gases pass through the SCR, varying proportions of GEM from 5% to 95% have been reported to convert into GOM [54,55]. Besides, the ammonia injection into flue gases before SCR might promote gaseous Hg adsorption onto fly ash [56,57]. These processes potentially fractionate Hg isotopes among different Hg species in SCR.

Sun et al. [35] developed a CFPP kinetic MDF model for Hg species in flue gases before APCDs by treating Hg isotope fractionation between Hg species as two independent, consecutive Rayleigh fractionation systems: homogeneous gaseous oxidation of GEM to GOM, and heterogeneous gas-particle conversion of GOM to PBM. This model assumes all transformation and isotope fractionation between Hg forms happen in flue gases before APCD, and predicts that GEM in the flue gases is significantly enriched in heavy Hg isotopes compared to GOM and PBM. δ^{202}Hg values of GEM, GOM and PBM can be calculated if the ratio of GEM:GOM:PBM in flue gases before APCD and δ^{202}Hg of feed coal are known. However, due to technic constrains (e.g., high temperature, high percentage of PBM that affect the Hg forms of the sampling flue gas and frequently blocked the sampling device), we can not sample the Hg forms in flue gases before ESPs. Lignite is commonly lacked of halogen elements (Cl, Br), most of Hg in flue gases before APCD is in the form of GEM [53,55]. Using the previously reported mean GEM:GOM:PBM = 79%:13%:7% in the flue gases before APCD(same

combination as this study) from one CFPP that fed by Chinese lignite [55], we calculated that the δ^{202}Hg values of GEM, GOM and PBM are higher than feed coal (−2.04 ± 0.25‰, 1SD) by +0.13 ± 0.02‰ (1SD), −0.27 ± 0.17‰ (1SD) and −0.83 ± 0.28‰ (1SD) using the CFPP kinetic MDF model of Sun et al. [35]. The predicted δ^{202}Hg value of PBM is −2.87 ± 0.38‰ (1SD), which is slightly lower than observed value of fly ash (−2.22 ± 0.13‰, 1SD). This small discrepancy might relate to equilibrium speciated Hg isotope fractionation in flue gases before APCDs. Both kinetic and equilibrium reactions between Hg species could occur in CFPP flue gases [58,59]. In contrast to kinetic reactions, equilibrium reactions between Hg forms tend to enrich heavy Hg isotopes in oxidized Hg species [58–60]. Alternatively, speciated Hg transformation in flue gases of SCR (e.g., oxidation of GEM to GOM, GOM sorption onto ammonia aerosols and fly ash) possibly fractionate Hg isotope as well. Lastly, Hg isotope composition of fly ash might not only represent that of PBM. Small fractions of GEM and GOM might adsorb onto the surface of fly ash [55]. All these processes possibly increase the δ^{202}Hg value of fly ash, and make the fly ash and feed coal indistinguishable in δ^{202}Hg.

3.6. Hg isotope MDF of Hg forms (GOMi, GEMi) in flue gases before WFGD

Relative to feed coal, GOMi (−1.34 ± 0.42‰, 1SD) and GEMi (−0.59 ± 0.31‰, 1SD) in the flue gases at inlet of WFGD are significantly enriched heavy Hg isotopes by 0.70 ± 0.49‰ (1SD) and 1.45 ± 0.39‰ (1SD) in δ^{202}Hg, respectively. As discussed above, the CFPP kinetic MDF model of Sun et al. [35] only predicts a δ^{202}Hg shift of −0.27 ± 0.17‰ (1SD), +0.13 ± 0.02‰ (1SD), respectively, for GOM and GEM in flue gases before APCDs relative to feed coal, using a GEM:GOM:PBM ratio of 79%:13%:7%. This implies that significant Hg isotope MDF might happen in SCR and/or ESPs. Regardless of exact mechanisms, if we assume speciated Hg isotope fractionation in flue gases before WFGD also follow the CFPP kinetic MDF model of Sun et al. [35] our measured GEM:GOM:PBM ratio (19%:29%:52%, assuming Hg in fly ash as PBM) would give a δ^{202}Hg shift of +0.88 ± 0.18‰ (1SD), +0.26 ± 0.34‰ (1SD) and −0.47 ± 0.19‰ (1SD) for GEM, GOM and PBM, respectively, relative to feed coal. These predicted δ^{202}Hg shifts for Hg species are slightly lower (0.3-0.5‰ in mean values) but are indistinguishable from those measured in samples, suggesting similar kinetic Hg isotope fractionation occurs in flue gases of SCR and/or ESPs as well. As reported previously, Hg transformation in coal combustion flue gases are dominantly kinetically controlled [58,59].

3.7. Hg isotope MDF of WFGD products and Hg forms(GEM, GOM) of flue gases after WFGD

After passing through WFGD, δ^{202}Hg in GEMo (0.54 ± 0.25‰, 1SD) and GOMo (−0.34 ± 0.13‰, 1SD) are elevated by 1.13 ± 0.39‰ (1SD) and 1.00 ± 0.44‰ (1SD), respectively, relative to GEMi and GOMi before WFGD. It suggests that Hg forms incorporated into the desulfurization gypsum and waste water are significantly enriched in light Hg isotopes. As expected, our ten WFGD gypsum samples (−2.18 ± 0.19‰, 1SD) and one WFGD waste water sample (−2.09 ± 0.04‰, 1SD) have very negative δ^{202}Hg values. Gypsum is slightly depleted (0.15‰ in δ^{202}Hg, $p > 0.10$) in the heavy Hg isotopes compared to feed coal, similar to the study of Sun et al. [36] WFGDs are thought to predominantly sequestrate GOM in the flue gases into desulfurization products (gypsum and waste water). The amounts of Hg in the flue gases at the inlet of WFGDs are 165 kg/y (1SD) containing 64 kg/y (1SD) of GEM, 101 kg/y (1SD) of GOM and 0.11 kg/y (1SD) of PBM. After desulfurization of flue gases in WFGD, the amounts of Hg in the flue gases are reduced to 60.3 kg/y (1SD) containing 53.6 kg/y (1SD) of GEM, 6.7 kg/y (1SD) of GOM and 0.05 kg/y (1SD) of PBM (Table S3). Therefore, 16% of GEM (10 kg/y), 93% of GOM (95 kg/y) and 55% of PBM (0.06 kg/y) were removed. Hg in limestone and fresh processing water are very low, and their Hg contributions to the whole CFPP is therefore negligible.

The dissolution of GOM into limestone slurry enriches heavy Hg isotopes in residual GOM. The outlet residual GOMo increases by 1.0‰ relative to inlet initial GOMi at 95% dissolution of GOMi. GEM is hardly soluble in water, its 16% reduction in WFGD might relate to the absorption and/or oxidation at the surface of limestone slurry aerosols. These observations support the dominantly kinetic Hg isotope MDF for GOM dissolution and GEM absorption and/or oxidation in WFGD, with reaction products enriching faster, lighter Hg isotopes. If we assume both GEM absorption and/or oxidation and GOM dissolution follow Rayleigh isotope fractionation, the fractionation factors for both reactions ($\alpha_{GEMoxidation}$ and $\alpha_{GOMdissolution}$) can be calculated, which are 0.9934 ± 0.0023 (1SD) and 0.9996 ± 0.0002 (1SD). Fig. S1 show that modeled δ^{202}Hg values of outlet residual GEM (reactant) and cumulative oxidized Hg (product) during GEM absorption and/or oxidation (A), and outlet residual GOM (reactant) and cumulative GOM (product) during GOM dissolution (B) using the above calculated $\alpha_{GEMoxidation}$ and $\alpha_{GOMdissolution}$ values. The gypsum and waste water in WFGD likely represent cumulative products of both GEM oxidation and GOM dissolution. The δ^{202}Hg values of cumulative products of GEM oxidation at 16% transformation of GEMi is −6.7 ± 2.1‰ (1SD), and the δ^{202}Hg cumulative products of GOM dissolution at 93% dissolution of GOMi is −1.4‰ ± 0.4‰ (1SD). According to Hg amounts of GEM (10 kg/y) and GOM (95 kg/y) retained in WFGD, we calculate that the weighted δ^{202}Hg of cumulative products is −1.9 ± 0.4‰ (1SD). This value is statistically same to the measured gypsum δ^{202}Hg of −2.18‰ ± 0.19‰ (1SD) within the uncertainty.

3.8. Comparison with atmospheric observations

Mercury isotope composition of atmospheric samples including air, rainfall and snowfall has been measured in North America, Europe and China [37,38,42,43,61–66]. In general, the total gaseous Hg (TGM = GEM + GOM, GEM > 90%) is enriched in the heavy isotopes (δ^{202}Hg = 0.51 ± 0.41‰, 1SD) and depleted odd isotopes (Δ^{199}Hg = −0.21 ± 0.06‰, 1SD)[37,43,61,62,64] compared to precipitation Hg (mainly GOM and PBM) (δ^{202}Hg = −0.87 ± 1.07‰, Δ^{199}Hg = 0.36 ± 0.30‰, 1SD) (Fig. 4) [38,42–63,65,66]. GEM in coal combustion flue gases is consistently enriched heavy Hg isotopes than GOM and PBM in our case study of CFPP equiped with SCR + ESP + WFGD. This fractioantion trend is also predicted by kinetic MDF model of Sun et al. [35] for CFPP equipped with ESP + WFGD. Using the world coal average δ^{202}Hg (−1.16 ± 0.79‰, 1SD) as a benchmak [29], the emitted GEM, GOM and PBM would be around 1.4‰, 0.5‰ and −1.3‰, respectively, using our observed MDF shifts between feed coal and speciated Hg emissions. Meanwhile, the CFPP kinetic MDF model of Sun et al. [35] predicts a δ^{202}Hg value of around −0.2‰, −1.1‰ and −1.7‰, respectively, for emitted GEM, GOM and PBM (Fig. 4). The δ^{202}Hg fractionation ranges of both GEM (−0.2‰ to 1.4‰) and GOM/PBM (−1.7‰ to 0.5‰) overlap most of global atmospehric Hg isotope observations. However, atmopsheric transformation of Hg species (e.g., oxidation, reduction, deposition) could fractionate speciated Hg as well. For example, Demers et al. [62] and Enrico et al. [67] observed >2.0‰ fractionation between forest foliage/vegetation and ambient air TGM. The large Δ^{199}Hg difference between coal Hg emissions and atmospheric samples might be attributed to photoreduction of atmospheric oxidized Hg species [12,43,66].

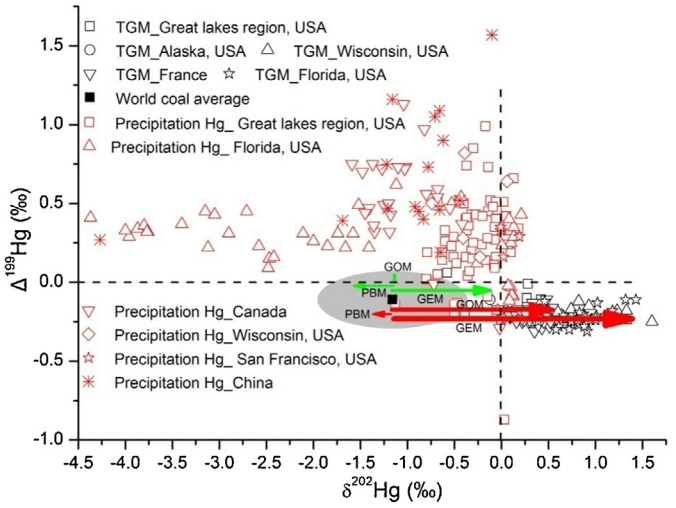

Fig. 4. Comparison of δ^{202}Hg and Δ^{199}Hg between Hg species in coal combustion flue gases and previously reported atmospheric samples. Black square represents the world coal, which is used as a benchmark to calculate δ^{202}Hg of Hg species emitted from CFUB. The gray ellipse indicates the mean ± 1SD variation ranges of δ^{202}Hg and Δ^{199}Hg in world coal. The red arrows show the δ^{202}Hg shifts of GEM (+2.6‰), GOM (+1.7‰) and PBM (−0.2‰, represented by fly ash) relative to world coal, assuming they have the same δ^{202}Hg shifts as in the present study. The green arrows show the δ^{202}Hg shifts of GEM (+1.0‰), GOM (+0.05‰) and PBM (−0.5‰,) relative to world coal, using the CFUB kinetic MDF model of Sun et al. [35]. TGM: Great lake regions, USA [43]; Alaska, USA [64]; Wisconsin, USA [62]; France [61]; Florida, USA [37]. Precipitation Hg: Great lake regions, USA [42,43]; Florida, USA [38]; Canada [66]; Wisconsin, USA [61]; San Francisco, USA [63]; China [65]. (For interpretation of the references to colour in this figure legend, the reader is referred to the web version of this article.)

4. Conclusions

In this study, we present the first speciated Hg isotope data of coal combustion flue gases from a typical Chinese CFPP fed by lignite. We confirm the speculations of Sun et al. [35,36] that different Hg forms have distinguishable δ^{202}Hg values and GEM is enriched heavy Hg isotopes relative to GOM and PBM. This information is critically important for near-field (GOM and PBM) and far-field (GEM) tracing of Hg emitted from coal-fired power plants. Relative to feed lignite, the emitted GEM and GOM are shifted by as large as 1.7–2.6‰ in δ^{202}Hg. These shifts should be considered in linking isotope composition of environment Hg receptors to coal combustion Hg emissions. Following Hg emissions from CFPP, atmospheric Hg transformation and Hg exchange at the critical boundaries (e.g., atmosphere and land) could fractionate Hg forms as well [43,62,66]. Reliable source Hg tracing should take into account of all underlying Hg isotope fractionation occurring pre- and post-Hg emissions.

While our study only concerns lignite-fed CFPP equipped with SCR + ESP + WFGD, CFPPs that fed by other types of coal (bituminous coal, anthracite) and equipped with other common APCD (e.g. ESP + WFGD, fabric filter + WFGD) combinations are needed to measure speciated Hg isotope as well in the future. We expect several widely applicable CFPP Hg isotope fractionation models can be constructed, in a similar way as Rayleigh isotope fractionation [35,36]. These models could be used to predict Hg isotope signatures of emitted Hg species of CFPPs using only coal Hg isotope composition and other traditional parameters (e.g., APCD Hg removal efficiency, ratio of Hg species in flue gases). Finally, apart from coal combustion flue gases, Hg isotope analysis of co-located ambient air and precipitation would be necessary to understand the Hg isotope fractionation pathways from feed coal to coal combustion flue gases and finally to atmospheric Hg.

Acknowledgments

This research was financed by the National Natural Science Foundation of China (41372360; 41573006; 41602167) and the Anhui Provincial Natural Science Foundation (1608085QD73). We thank the editor and anonymous reviewers for their thoughtful comments, which significantly improve the quality of this paper.

Appendix A. Supplementary data

Supplementary data associated with this article can be found, in the online version, at http://dx.doi.org/10.1016/j.jhazmat.2017.01.014.

References

[1] N. Pirrone, S. Cinnirella, X. Feng, R.B. Finkelman, H.R. Friedli, J. Leaner, R. Mason, A.B. Mukherjee, G.B. Stracher, D.G. Streets, K. Telmer, Global mercury emissions to the atmosphere from anthropogenic and natural sources, Atmos. Chem. Phys. 10 (2010) 5951–5964.
[2] D.G. Streets, M.K. Devane, Z. Lu, T.C. Bond, E.M. Sunderland, D.J. Jacob, All-time releases of mercury to the atmosphere from human activities, Environ. Sci. Technol. 45 (2011) 10485–10491.
[3] E. Bagnato, G. Tamburello, G. Avard, M. Martinez-Cruz, M. Enrico, X. Fu, M. Sprovieri, J.E. Sonke, Mercury fluxes from volcanic and geothermal sources: an update, Geol. Soc. Lond., Spec. Publ. 410 (2014).
[4] W.H. Schroeder, J. Munthe, Atmospheric mercury–an overview, Atmos. Environ. 32 (1998) 809–822.
[5] R.P. Mason, W.F. Fitzgerald, F.M.M. Morel, The biogeochemical cycling of elemental mercury: anthropogenic influences, Geochim. Cosmochim. Acta 58 (1994) 3191–3198.
[6] C. Seigneur, K. Vijayaraghavan, K. Lohman, P. Karamchandani, C. Scott, Global source attribution for mercury deposition in the United States, Environ. Sci. Technol. 38 (2004) 555–569.
[7] C.H. Lamborg, C.R. Hammerschmidt, K.L. Bowman, G.J. Swarr, K.M. Munson, D.C. Ohnemus, P.J. Lam, L.-E. Heimburger, M.J.A. Rijkenberg, M.A. Saito, A global ocean inventory of anthropogenic mercury based on water column measurements, Nature 512 (2014) 65–68.
[8] H.M. Amos, J.E. Sonke, D. Obrist, N. Robins, N. Hagan, H.M. Horowitz, R.P. Mason, M. Witt, I.M. Hedgecock, E.S. Corbitt, E.M. Sunderland, Observational and modeling constraints on global anthropogenic enrichment of mercury, Environ. Sci. Technol. 49 (2015) 4036–4047.
[9] E.G. Pacyna, J.M. Pacyna, K. Sundseth, J. Munthe, K. Kindbom, S. Wilson, F. Steenhuisen, P. Maxson, Global emission of mercury to the atmosphere from anthropogenic sources in 2005 and projections to 2020, Atmos. Environ. 44 (2010) 2487–2499.
[10] J.D. Blum, L.S. Sherman, M.W. Johnson, Mercury isotopes in earth and environmental sciences, Annu. Rev. Earth Planet. Sci. 42 (2014) 249–269.
[11] R. Yin, X. Feng, X. Li, B. Yu, B. Du, Trends and advances in mercury stable isotopes as a geochemical tracer, Anal. Chem. 2 (2014) 1–10.
[12] J.E. Sonke, A global model of mass independent mercury stable isotope fractionation, Geochim. Cosmochim. Acta 75 (2011) 4577–4590.
[13] J.E. Sonke, J.D. Blum, Advances in mercury stable isotope biogeochemistry, Chem. Geol. 336 (2013) 1–4.
[14] B.A. Bergquist, J.D. Blum, Mass-dependent and -independent fractionation of Hg isotopes by photoreduction in aquatic systems, Science 318 (2007) 417–420.
[15] C.H. Rose, S. Ghosh, J.D. Blum, B.A. Bergquist, Effects of ultraviolet radiation on mercury isotope fractionation during photo-reduction for inorganic and organic mercury species, Chem. Geol. 405 (2015) 102–111.
[16] W. Zheng, H. Hintelmann, Mercury isotope fractionation during photoreduction in natural water is controlled by its Hg/DOC ratio, Geochim. Cosmochim. Acta 73 (2009) 6704–6715.
[17] W. Zheng, H. Hintelmann, Nuclear field shift effect in isotope fractionation of mercury during abiotic reduction in the absence of light, J. Phys. Chem. A 114 (2010) 4238–4245.
[18] K. Kritee, J.D. Blum, J.R. Reinfelder, T. Barkay, Microbial stable isotope fractionation of mercury: a synthesis of present understanding and future directions, Chem. Geol. 336 (2013) 13–25.
[19] P. Rodríguez-González, V.N. Epov, R. Bridou, E. Tessier, R. Guyoneaud, M. Monperrus, D. Amouroux, Species-specific stable isotope fractionation of mercury during Hg(II) methylation by an anaerobic bacteria (Desulfobulbus propionicus) under dark conditions, Environ. Sci. Technol. 43 (2009) 9183–9188.
[20] V. Perrot, M. Jimenez-Moreno, S. Berail, V.N. Epov, M. Monperrus, D. Amouroux, Successive methylation and demethylation of methylated mercury species (MeHg and DMeHg) induce mass dependent fractionation of mercury isotopes, Chem. Geol. 355 (2013) 153–162.
[21] V. Perrot, R. Bridou, Z. Pedrero, R. Guyoneaud, M. Monperrus, D. Amouroux, Identical Hg isotope mass dependent fractionation signature during

methylation by sulfate-reducing bacteria in sulfate and sulfate-free environment, Environ. Sci. Technol. 49 (2015) 1365–1373.
[22] K. Kritee, T. Barkay, J.D. Blum, Mass dependent stable isotope fractionation of mercury during mer mediated microbial degradation of monomethylmercury, Geochim. Cosmochim. Acta 73 (2009) 1285–1296.
[23] P. Chandan, S. Ghosh, B.A. Bergquist, Mercury isotope fractionation during aqueous photoreduction of monomethylmercury in the presence of dissolved organic matter, Environ. Sci. Technol. 49 (2015) 259–267.
[24] W. Zheng, D. Foucher, H. Hintelmann, Mercury isotope fractionation during volatilization of Hg(0) from solution into the gas phase, J. Anal. Atomic Spectrom. 22 (2007) 1097–1104.
[25] N. Estrade, J. Carignan, J.E. Sonke, O.F.X. Donard, Mercury isotope fractionation during liquid-vapor evaporation experiments, Geochim. Cosmochim. Acta 73 (2009) 2693–2711.
[26] S. Ghosh, E.A. Schauble, G. Lacrampe Couloume, J.D. Blum, B.A. Bergquist, Estimation of nuclear volume dependent fractionation of mercury isotopes in equilibrium liquid–vapor evaporation experiments, Chem. Geol. 336 (2013) 5–12.
[27] J.G. Wiederhold, C.J. Cramer, K. Daniel, I. Infante, B. Bourdon, R. Kretzschmar, Equilibrium mercury isotope fractionation between dissolved Hg(II) species and thiol-bound Hg, Environ. Sci. Technol. 44 (2010) 4191–4197.
[28] M. Jiskra, J.G. Wiederhold, B. Bourdon, R. Kretzschmar, Solution speciation controls mercury isotope fractionation of Hg(II) sorption to goethite, Environ. Sci. Technol. 46 (2012) 6654–6662.
[29] R. Sun, J.E. Sonke, G. Liu, Biogeochemical controls on mercury stable isotope compositions of world coal deposits: a review, Earth Sci. Rev. 152 (2016) 1–13.
[30] R.S. Smith, J.G. Wiederhold, A.D. Jew, G.E. Brown Jr., B. Bourdon, R. Kretzschmar, Small-scale studies of roasted ore waste reveal extreme ranges of stable mercury isotope signatures, Geochim. Cosmochim. Acta 137 (2014) 1–17.
[31] R. Yin, X. Feng, J.P. Hurley, D.P. Krabbenhoft, R.F. Lepak, R. Hu, Q. Zhang, Z. Li, X. Bi, Mercury isotopes as proxies to identify sources and environmental impacts of mercury in sphalerites, Sci. Rep 6 (2016) 18686.
[32] V. Perrot, M.V. Pastukhov, V.N. Epov, S. Husted, O.F.X. Donard, D. Amouroux, Higher mass-Independent isotope fractionation of methylmercury in the pelagic food web of Lake Baikal (Russia), Environ. Sci. Technol. 46 (2012) 5902–5911.
[33] H. Hintelmann, S. Lu, High precision isotope ratio measurements of mercury isotopes in cinnabar ores using multi-collector inductively coupled plasma mass spectrometry, Analyst 128 (2003) 635–639.
[34] A. Biswas, J.D. Blum, B.A. Bergquist, G.J. Keeler, Z. Xie, Natural mercury isotope variation in coal deposits and organic soils, Environ. Sci. Technol. 42 (2008) 8303–8309.
[35] R. Sun, J.E. Sonke, L.-E. Heimbürger, H.E. Belkin, G. Liu, D. Shome, E. Cukrowska, C. Liousse, O.S. Pokrovsky, D.G. Streets, Mercury stable isotope signatures of world coal deposits and historical coal combustion emissions, Environ. Sci. Technol. 48 (2014) 7660–7668.
[36] R. Sun, L.-E. Heimbürger, J.E. Sonke, G. Liu, D. Amouroux, S. Berail, Mercury stable isotope fractionation in six utility boilers of two large coal-fired power plants, Chem. Geol. 336 (2013) 103–111.
[37] J.D. Demers, L.S. Sherman, J.D. Blum, F.J. Marsik, J.T. Dvonch, Coupling atmospheric mercury isotope ratios and meteorology to identify sources of mercury impacting a coastal urban-industrial region near Pensacola, Florida USA, Global Biogeochem. Cycles 29 (2015) 1689–1705.
[38] L.S. Sherman, J.D. Blum, G.J. Keeler, J.D. Demers, J.T. Dvonch, Investigation of local mercury deposition from a coal-Fired power plant using mercury isotopes, Environ. Sci. Technol. 46 (2012) 382–390.
[39] M. Derda, A. Grzegorz Chmielewski, J. Licki, Sulphur isotope compositions of components of coal and S-isotope fractionation during its combustion and flue gas desulphurization, Isotopes Environ. Health Stud. 43 (2007) 57–63.
[40] R. Ochoa Gonzalez, D. Weiss, Zinc isotope variability in three coal-fired power plants: a predictive model for determining isotopic fractionation during combustion, Environ. Sci. Technol. 49 (2015) 12560–12567.
[41] Q. Huang, J. Chen, W. Huang, P. Fu, B. Guinot, X. Feng, L. Shang, Z. Wang, Z. Wang, S. Yuan, H. Cai, L. Wei, B. Yu, Isotopic composition for source identification of mercury in atmospheric fine particles, Atmos. Chem. Phys. 16 (2016) 11773–11786.
[42] L.S. Sherman, J.D. Blum, J.T. Dvonch, L.E. Gratz, M.S. Landis, The use of Pb, Sr, and Hg isotopes in Great Lakes precipitation as a tool for pollution source attribution, Sci. Total Environ. 502 (2015) 362–374.
[43] L.E. Gratz, G.J. Keeler, J.D. Blum, L.S. Sherman, Isotopic composition and fractionation of mercury in great lakes precipitation and ambient air, Environ. Sci. Technol. 44 (2010) 7764–7770.
[44] A. D6784-02, Standard Test Method for Elemental, Oxidized, Particle-Bound and Total Mercury in Flue Gas Generated from Coal-Fired Stationary Sources (OntarioHydro Method), in, ASTM, International, West Conshohocken, PA, 2008.
[45] S. Tang, L. Wang, X. Feng, Z. Feng, R. Li, H. Fan, K. Li, Actual mercury speciation and mercury discharges from coal-fired power plants in Inner Mongolia, Northern China, Fuel 180 (2016) 194–204.
[46] R. Sun, M. Enrico, L.-E. Heimbürger, C. Scott, J. Sonke, A double-stage tube furnace—acid-trapping protocol for the pre-concentration of mercury from solid samples for isotopic analysis, Anal. Bioanal. Chem. 405 (2013) 6771–6781.
[47] J.D. Blum, B.A. Bergquist, Reporting of variations in the natural isotopic composition of mercury, Anal. Bioanal. Chem. 388 (2007) 353–359.
[48] R. Yin, X. Feng, J. Chen, Mercury stable isotopic compositions in coals from major coal producing fields in China and their geochemical and environmental implications, Environ. Sci. Technol. 48 (2014) 5565–5574.
[49] J.G. Wiederhold, R.S. Smith, H. Siebner, A.D. Jew, G.E. Brown, B. Bourdon, R. Kretzschmar, Mercury isotope signatures as tracers for hg cycling at the new idria Hg mine, Environ. Sci. Technol. 47 (2013) 6137–6145.
[50] R. Yin, X. Feng, J. Wang, P. Li, J. Liu, Y. Zhang, J. Chen, L. Zheng, T. Hu, Mercury speciation and mercury isotope fractionation during ore roasting process and their implication to source identification of downstream sediment in the Wanshan mercury mining area, SW China, Chem. Geol. 336 (2013) 72–79.
[51] J.E. Gray, M.J. Pribil, P.L. Higueras, Mercury isotope fractionation during ore retorting in the Almadén mining district, Spain, Chem. Geol. 357 (2013) 150–157.
[52] S. Li, C.-M. Cheng, B. Chen, Y. Cao, J. Vervynckt, A. Adebambo, W.-P. Pan, Investigation of the relationship between particulate-Bound mercury and properties of fly ash in a full-Scale 100 MWe pulverized coal combustion boiler, Energ. Fuel 21 (2007) 3292–3299.
[53] L. Zhang, S. Wang, Y. Meng, J. Hao, Influence of mercury and chlorine content of coal on mercury emissions from coal-fired power plants in China, Environ. Sci. Technol. 46 (2012) 6385–6392.
[54] C.W. Lee, S.D. Serre, Y. Zhao, S.J. Lee, T.W. Hastings, Mercury oxidation promoted by a selective catalytic reduction catalyst under simulated powder river basin coal combustion conditions, J. Air Waste Manag. Assoc. 58 (2008) 484–493.
[55] S.X. Wang, L. Zhang, G.H. Li, Y. Wu, J.M. Hao, N. Pirrone, F. Sprovieri, M.P. Ancora, Mercury emission and speciation of coal-fired power plants in China, Atmos. Chem. Phys. 10 (2010) 1183–1192.
[56] Y. Gao, Z. Zhang, J. Wu, L. Duan, A. Umar, L. Sun, Z. Guo, Q. Wang, A critical review on the heterogeneous catalytic oxidation of elemental mercury in flue gases, Environ. Sci. Technol. 47 (2013) 10813–10823.
[57] J.R. Turner, S. Choné, M.P. Duduković, Ammonia/flyash interactions and their impact on flue gas treatment technologies, Chem. Eng. Sci. 49 (1994) 4315–4325.
[58] T.K. Gale, B.W. Lani, G.R. Offen, Mechanisms governing the fate of mercury in coal-fired power systems, Fuel Process. Technol. 89 (2008) 139–151.
[59] Y. Zhuang, J.S. Thompson, C.J. Zygarlicke, J.H. Pavlish, Development of a mercury transformation model in coal combustion flue gas, Environ. Sci. Technol. 38 (2004) 5803–5808.
[60] E.A. Schauble, Role of nuclear volume in driving equilibrium stable isotope fractionation of mercury, thallium, and other very heavy elements, Geochim. Cosmochim. Acta 71 (2007) 2170–2189.
[61] X. Fu, L.-E. Heimburger, J.E. Sonke, Collection of atmospheric gaseous mercury for stable isotope analysis using iodine- and chlorine-impregnated activated carbon traps, J. Anal. Atomic Spectrom. 29 (2014) 841–852.
[62] J.D. Demers, J.D. Blum, D.R. Zak, Mercury isotopes in a forested ecosystem: implications for air-surface exchange dynamics and the global mercury cycle, Global Biogeochem. Cycles 27 (2013) 222–238.
[63] P.M. Donovan, J.D. Blum, D. Yee, G.E. Gehrke, M.B. Singer, An isotopic record of mercury in San Francisco Bay sediment, Chem. Geol. 349–350 (2013) 87–98.
[64] L.S. Sherman, J.D. Blum, K.P. Johnson, G.J. Keeler, J.A. Barres, T.A. Douglas, Mass-independent fractionation of mercury isotopes in Arctic snow driven by sunlight, Nat. Geosci. 3 (2010) 173–177.
[65] Z. Wang, J. Chen, X. Feng, H. Hintelmann, S. Yuan, H. Cai, Q. Huang, S. Wang, F. Wang, Mass-dependent and mass-independent fractionation of mercury isotopes in precipitation from Guiyang, SW China, C. R. Geosci. 347 (2015) 358–367.
[66] J. Chen, H. Hintelmann, X. Feng, B. Dimock, Unusual fractionation of both odd and even mercury isotopes in precipitation from Peterborough, ON, Canada, Geochim. Cosmochim. Acta 90 (2012) 33–46.
[67] M. Enrico, G.L. Roux, N. Marusczak, L.-E. Heimbürger, A. Claustres, X. Fu, R. Sun, J.E. Sonke, Atmospheric mercury transfer to peat bogs dominated by gaseous elemental mercury dry deposition, Environ. Sci. Technol. 50 (2016) 2405–2412.